Ultrasonics Sonochemistry 18 (2011) 1038–1042

Contents lists available at ScienceDirect

Ultrasonics Sonochemistry

journal homepage: www.elsevier.com/locate/ultsonch

Rapid growth of magnetite nanoplates by ultrasonic irradiation at low temperature

J.P. Cheng *, R. Ma, D. Shi, F. Liu, X.B. Zhang

State Key Laboratory of Silicon Materials, Department of Materials Science and Engineering, Zhejiang University, Hangzhou 310027, China

ARTICLE INFO

Article history:
Received 18 June 2010
Received in revised form 2 December 2010
Accepted 23 December 2010
Available online 31 December 2010

Keywords:
Magnetite
Two-dimensional
Nanoplate
Ultrasonic irradiation
Magnetic property

ABSTRACT

Two-dimensional plate-like Fe_3O_4 nanocrystals were synthesized by a facile method using ultrasonic irradiation in aqueous solution at low temperature without protection from oxygen. The crystals were characterized by X-ray diffraction, scanning electron microscopy, transmission electron microscopy, X-ray photoelectron spectroscopy, and Fourier Transform infrared spectroscopy. The products subjected to ultrasound showed a two-dimensional morphology. The results obtained indicate that the morphologies of the magnetite crystals depend more on the ultrasonic irradiation than on the growth temperature. The thickness and width of the crystals increased with increasing temperature of the reaction medium. In addition, the magnetic hysteresis loop of the magnetite nanoplates was obtained at room temperature.

1. Introduction

Recently, the synthesis of magnetite nanostructures has become a particularly important issue and is attracting growing interest. Different from bulk materials, they usually display unique properties due to their small particle size and large surface area [1], and have potential applications in many fields, such as magnetic fluids [2], magnetic resonance imaging [3], adsorbents for environmental engineering [4] and biotechnologies [5]. Up to now, researchers have proposed several synthesis approaches, such as co-precipitating ferrous and ferric ions in solution [6,7], the sol–gel method [8], hydrothermal synthesis [5,9], thermal decomposition [10,11], solvothermal methods [12–15], microwave-assisted methods [5,16] and the polyol process [12,17]. However, most of these approaches contain multi-step synthetic processes or protection from oxygen, involving unfavorably high growth temperatures (at least 100 °C, even higher than 600 °C) and long reaction times.

The magnetic properties of nanomaterials are greatly dependent on the particle size and morphology [18]. When the size of the magnetic particles is adequately small, each particle can be a single magnetic domain [19] and exhibit superparamagnetic properties [20]. A great deal of effort has gone into the fabrication of extremely small magnetite crystals with different morphologies, such as nanoparticles [3], nanorods [11,15,21], nanowires [22,23], nanoplates [1,9,12,13,16,24] and hierarchical nanostructures [5,25]. However, most of these structures are one-dimensional or three-dimensional [11,15,22,23]. Compared with these structures, two-dimensional (2-D) nanocrystals will have a large specific surface area [26,27] and will display magnetic anisotropism. Only a few groups have reported the synthesis of 2-D magnetite nanocrystals. Zhou et al. applied a microwave-assisted route to prepare hexagonal magnetite nanoplates with a large average edge length up to 80 nm [16]. Though Zhang [9], Liu [13] and Zou [24] had devised a solvothermal method to fabricate 2-D magnetite nanocrystals, the reaction temperature was as high as 200 °C and the shortest reaction time was 12 h. Thus, the synthesis of 2-D magnetite nanoplates under moderate conditions with high efficiency has hardly been studied.

Ultrasonic irradiation has proven to be an effective method to synthesize magnetic nanoparticles [18,21,28–30]. Feng has synthesized cubic magnetite particles with a size of 11 nm using ultrasonic irradiation in water–ethanol solution at 50 °C for 1 h [29]. Mukh-Qasem synthesized a stable aqueous dispersion of magnetite particles using high-intensity ultrasound through the decomposition of $Fe(CO)_5$ [30]. The ultrasonic method can not only raise the reaction rate, but also make the reaction occur at low temperature because of the so called "cavitation" phenomenon. The transmission of high-frequency ultrasound in liquid could cause the formation, growth, and collapse of bubbles, and the rapid collapse of bubbles creates high temperature (about 5000 K), high pressure (about 20 MPa) and high cooling rate (about 10^{10} K/S) [29]. To the best of our knowledge, there are few reports on the synthesis of 2-D magnetite nanocrystals by ultrasonic irradiation.

Conventional magnetite synthesis always requires deoxygenated conditions and Fe^{2+}/Fe^{3+} molar ratio control. In this paper, we report a facile method to synthesize 2-D magnetite nanoplates by ultrasonic irradiation using $FeSO_4$ and NaOH as reagents at low

* Corresponding author. Tel./fax: +86 571 87951411.
E-mail address: chengjp@zju.edu.cn (J.P. Cheng).

1350-4177/$ - see front matter © 2010 Elsevier B.V. All rights reserved.
doi:10.1016/j.ultsonch.2010.12.008

temperature without deoxygenated conditions. The reagents used here are cheap, and the fabrication process is one step and easy to achieve in a short time. The magnetic properties of as-prepared magnetite nanocrystals have been also investigated.

2. Experimental

All the chemicals used in the present work were of analytical grade and used as received without further purification. Distilled water was used to prepare aqueous solution in the synthesis process.

In a typical procedure, 2.3353 g of $FeSO_4{\cdot}7H_2O$ was dissolved in 120 mL of water and it was named solution A. Separately, 0.672 g of NaOH and 6.89 g of NaAc were all dissolved in 80 mL of water to form a clear solution, labeled solution B. The solution B was initially kept at 80 °C or room temperature by a water bath, and then solution A was added dropwise into solution B under ultrasonic irradiation in the open air. Ultrasonic waves were generated from a titanium horn which was directly immersed into solution B, and the schematic diagram of the experimental setup was shown in Fig. 1. The output powder injected into the sample solution was found to be about 80 W judged from the panel in the ultrasonic generator (JY92-II, Ningbo Scientz Biotechnology Co., Ltd.). To avoid rapid increase of temperature in the reaction medium, the generated ultrasonic is triggered following a cycled periodic pulse. The width of the pulse in a period was 22 s. The duration of ultrasound was 20 s, and the resting time was 2 s.

During the addition of solution A, the reaction mixture was constantly subjected to the pulsed ultrasonic irradiation. After adding solution A, the mixture was changed into black suspension and the resulting suspension was allowed to cool down to room temperature naturally. The precipitate was separated by filtration, wished with distilled water and ethanol several times, and dried under vacuum 50 °C for hours. In this study, the reaction time was usually no more than 30 min. The products prepared from the initial solution at 80 °C and at room temperature were named as sample M1 and M2, respectively. For comparison, another sample named M3 was prepared by conventional mechanical stirring under 80 °C for 1 h using a similar procedure to that described above.

The crystallographic information of the products was obtained by X-ray diffraction (XRD) and the patterns were recorded on an X-ray diffractometer (X'Pert PRO) with Cu Kα radiation. The morphology and size of the particles were observed using a field emission scanning electron microscope (FE-SEM, Hitachi S-4800) and a transmission electron microscopy (TEM, Philips CM200). The products were also analyzed by X-ray photoelectron spectroscopy (XPS, Kratos AXIS Ultra DLD) and Fourier Transform infrared spectroscopy (FTIR, Bruker Vector 22). The magnetic properties were characterized by a vibrating sample magnetometer (VSM, Lakeshore 7407) at room temperature.

3. Results and discussion

Fig. 2 displays the XRD patterns of the three samples. According to PDF Cards 65-3107, the reflection peaks at the 2θ values of 18.3°, 30.1°, 35.4°, 37.1°, 43.1°, 53.4°, 57.0° and 62.6° can be indexed to the (1 1 1), (2 2 0), (3 1 1), (2 2 2), (4 0 0), (4 2 2), (5 1 1) and (4 4 0) planes of cubic magnetite, respectively. However, diffraction analysis alone cannot distinguish the cubic magnetite and maghemite because of their similarity in structure and lattice parameters. To further prove the existence of magnetite, XPS spectra were examined and are shown in Fig. 5. In curve *a*, for sample M1, the strong intensity and narrow width of diffraction peaks indicate that the resulting products are of good crystallinity. No diffraction peaks from other species can be detected, implying that all the precursors have been transformed into the magnetite phase. For sample M2 in curve *b*, a small peak located at $2\theta = 40.5°$ should be assigned to FeOOH. We deduce that it should be involved in the chemical reaction. However, only the most intense reflections (3 1 1 and 4 4 0) were observed in the curve *c* for sample M3, caused by small crystal size as well as poor crystallinity. From the XRD results, it can be concluded that the particle sizes of the samples synthesized under ultrasonic irradiation are larger than those synthesized under mechanical stirring [29], and the crystallinity of the magnetite phase could be greatly improved by ultrasonic irradiation.

SEM was used to observe the morphologies of the products and the corresponding micrographs are presented in Fig. 3. A highly aggregated morphology is illustrated in Fig. 3a, which depicts sample M1. The aggregate consist of 2-D nanoplates, having a thickness ranging from 10 to 20 nm and a lateral size between 50 and 90 nm. While decreasing the initial temperature to room temperature, the product also exhibits flatten particle morphology in Fig. 3b. These nanoparticles have facets ranging from 25 to 60 nm. Side views that are vertical to the SEM grid indicate that the thickness is between 5 and 10 nm. This means that changing the initial temperature of the solution does not generate morphological changes for products, but it can influence the size of the as-synthesized nanoplates. The size of the nanoplates increases with an increase in the growth temperature. The mean diameter of particles for sample

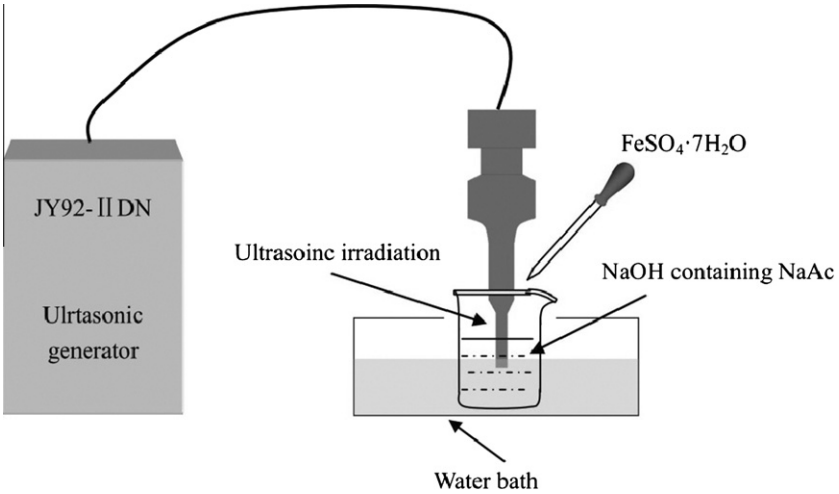

Fig. 1. Schematic diagram of the reaction setup.

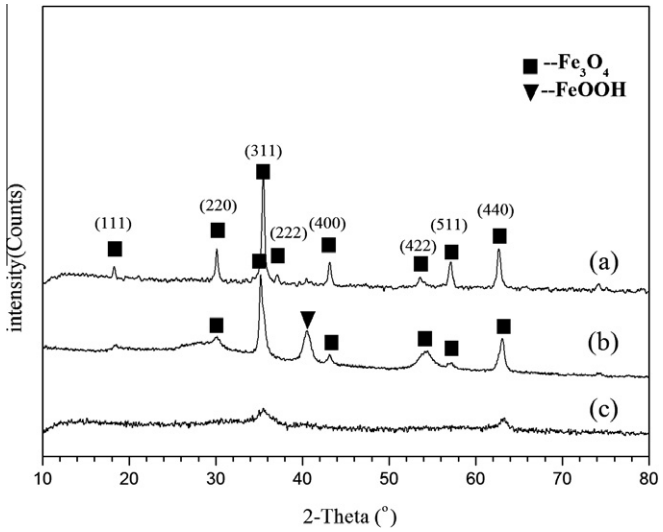

Fig. 2. XRD patterns of (a) M1 under ultrasonic treatment at 80 °C, (b) M2 under ultrasonic treatment at room temperature and (c) M3 under mechanical stirring at 80 °C.

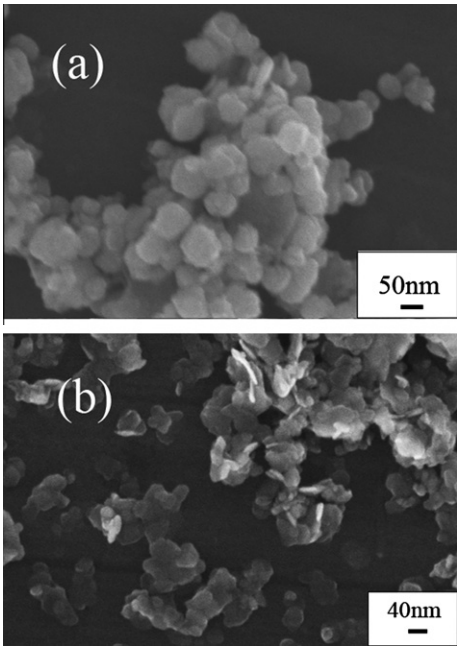

Fig. 3. SEM images of sample (a) M1 synthesized at 80 °C and (b) M2 at room temperature under ultrasonic irradiation.

M3 by SEM was about 15 nm, with uniform size and spherical shape (shown in the Supporting Information), which was much smaller than those under ultrasonic irradiation, consistent with XRD analysis.

To further investigate the morphologies and crystallographic features of the Fe_3O_4 nanoplates, TEM images are recorded in Fig. 4. Fig. 4a and b shows low magnification TEM images of sample M1 and M2, respectively. Selected area electron diffraction for each nanoplate indicated that they possess a single-crystal structure. From the image in Fig. 4b, these 2-D Fe_3O_4 flakes are homogeneous in thickness with sharp crystallographic edges. The morphology is thought to have developed naturally as a result of crystallographic habit.

More detailed structural information for sample M2 was examined by HRTEM analysis, as shown in Fig. 4c. Clear lattice fringes of

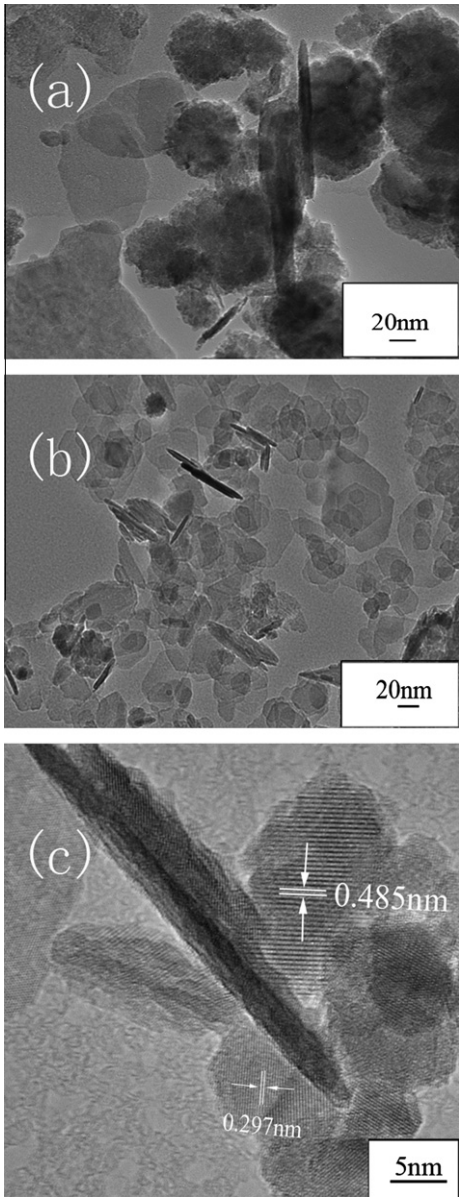

Fig. 4. TEM images for sample (a) M1, (b) M2 and HRTEM image of M2 (c).

Fe_3O_4 are obviously observed, indicting the single crystalline nature. The measured spacing of the crystallographic planes is about 0.48 nm and 0.29 nm for two individual crystals, which are close to the distances of (1 1 1) and (2 2 0) planes of magnetite crystals, respectively. The thickness of a nanoplate whose side view is vertical to the TEM electron beam in Fig. 4c was measured to be about 5 nm. It is thus considered that these Fe_3O_4 nanoplates are most likely to grow along [1 1 0] or [1 1 1] direction in our cases. Fe_3O_4 has well-defined magnetic axes along [1 1 0] and [1 1 1] directions. Our result is also consistent with the previous report [24].

Due to the proximate lattice parameters of magnetite and maghemite, it is hard to distinguish these two materials from each other alone by XRD. Further evidence of the formation of Fe_3O_4 was obtained from XPS. Fig. 5 shows XPS spectrum in the Fe 2p region of sample M1. The peak positions of Fe $2p_{3/2}$ and Fe $2p_{1/2}$ are at 711.7 and 724.7 eV, respectively. These values are consistent with those for Fe_3O_4 reported in the literature [31], which further confirms the composition of Fe_3O_4. Besides peak position, the appearance of a satellite peak for Fe $2p_{3/2}$ is also an important feature to discriminate magnetite and maghemite [32]. As seen in the

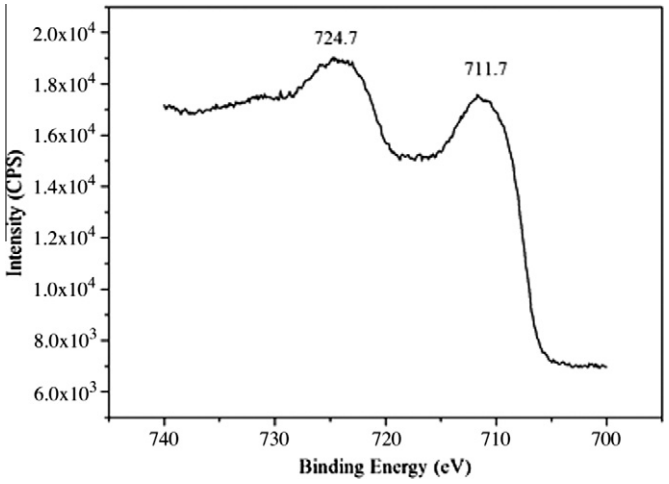

Fig. 5. XPS spectrum of sample M1 in the Fe 2p region.

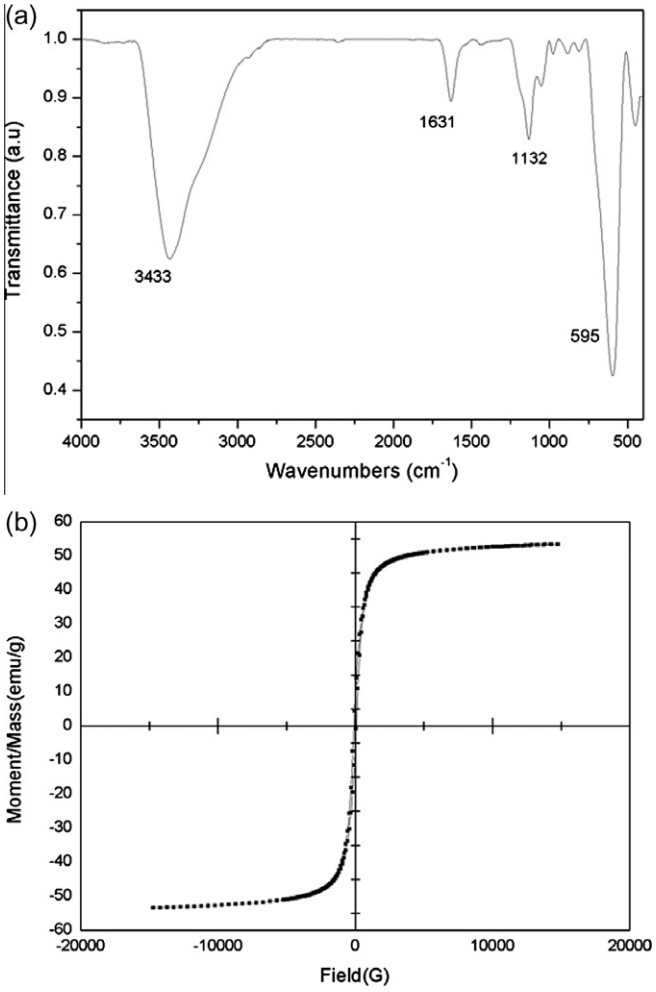

Fig. 6. FTIR spectrum (a) and magnetic hysteresis loop (b) of sample M1.

spectrum, the absence of a satellite peak further substantiates the formation of magnetite.

To understand the surface chemical composition of Fe_3O_4 nanocrystals, FTIR spectrum of sample M1 was examined and presented in Fig. 6a. The peak at 595 cm^{-1} is the stretching vibration due to the interactions of Fe–O–Fe in Fe_3O_4 and the intensity of the Fe–O–Fe absorption band is much strong here. The band centered at 3433 cm^{-1} can be assigned to hydrogen bonded O–H stretching vibration arising from surface hydroxyl groups on the nanoplates and adsorbed water. The absorption band located at 1631 cm^{-1} is due to a C=O vibration, and is due to the surface absorbed carbonyl group from the presence of NaAc. The presence of sulfate was also confirmed by the S–O stretching at 1132 cm^{-1}, which came from the residual salts.

The magnetization loop of sample M1 is shown in Fig. 6b. The saturation magnetizations (Ms) and coercivity values for sample M1 are about 54 emu/g and 83O e, respectively. The value of Ms for sample M1 is relatively low compared to its bulk value of 92 emu/g [33]. Although the detailed reasons are not clear, this phenomenon may originate from two parts. One is the nano-sized effect for ultrafine magnetic particles. The Ms will decrease due to the small size of the final product [6,7,24]. The other is that contamination of the sample could cause a slight loss of saturation magnetization [6].

From above results, we conclude that there are two factors that have great influence on the magnetite crystals. One is reverse precipitation. In the present case, the acidic ferrous solution was added dropwise to a large amount of basic solution, which has been referred to as reverse precipitation [18,34]. The pH values of the reaction medium could be kept high enough to make all the components precipitate completely as hydroxides, allowing homogeneous co-precipitation to occur within individual droplets [18,34,35]. Otherwise, the magnetite nanoparticles fabricated by sonochemical oxidation of $Fe(OH)_2$ obtained by adding alkaline solution to aqueous ferrous solution were generally larger in size [18]. Thus, nanoscaled magnetite particles with average size about 15 nm were obtained from the reaction medium under mechanical stirring (shown in the Supporting Information). When the reaction solution was subjected to ultrasonic waves, much smaller nanoparticles could be formed due to the effective agitation and in situ formation of active species via cavitational collapse [21,28–30]. The other factor is the oxidation rate of $Fe(OH)_2$. Aqueous $FeSO_4$ can react with NaOH to yield $Fe(OH)_2$ which is readily converted to $Fe(OH)_3$ by oxidation with dissolved oxygen in an alkaline medium. When the oxidation of $Fe(OH)_2$ takes place under air, magnetite with a small amount of FeOOH is mainly produced [18,35]. As the oxidation rate of $Fe(OH)_2$ is increased, the size of the magnetite would decrease significantly [35]. Because the amount of dissolved oxygen in water decreases with increasing temperature, the oxygen rate for sample M1 was slower than that for sample M2 and pure-phased magnetite product was thus obtained at 80 °C. In the solution subjected to ultrasonic waves, water molecules are thermally decomposed to generate hydrogen atom and hydroxyl radical, which can recombine to form hydrogen, hydrogen peroxide, and water [21,29]. Higher amounts of hydrogen peroxide would be thus formed when oxygen or air is dissolved in water [18]. The magnetite nanoparticles would be produced through the oxidation of $Fe(OH)_2$ by hydrogen peroxide. Thus, the formation rate of magnetite nuclei under ultrasonic irradiation was accelerated when compared with that under mechanical stirring [29].

When the precursor solution is exposed to ultrasonic irradiation, it will provide enough energy for the quick generation of primary magnetite crystal nuclei [21]. The high oxidation rate by ultrasonic irradiation as well as reverse precipitation would rapidly produce extremely small magnetite nuclei, at least smaller than the 15 nm size observed in the mechanical stirring case. The intense microscopic turbulence and micro-jets generated from the collapse of bubbles consequently inhibit the rapid growth of Fe_3O_4 nuclei. The reason for the particle size of the sample synthesized under ultrasonic was larger than those under mechanical stirring is caused by the consequent crystal growth [29], *i.e.*

attributing to cooperation of oriented aggregation and Ostwald ripening. To decrease the high surface free energy, the adjacent nuclei in suspension would be self-assembled and oriented by attaching one-by-one toward the formation of large crystals [36–40], which is chiefly related to the intrinsic crystal structure of magnetite and the well-defined magnetization axes [39,41]. Several smaller nuclei were perfectly aligned, forming a single crystal during oriented attachment. Ostwald ripening is also active alongside oriented attachment and smooth crystal surface is perhaps a clear indication of diffusion and fusion [39]. Thus, these small nuclei assembled along the [1 1 0] or [1 1 1] direction and larger Fe_3O_4 nanoplates were formed by the mechanism of spontaneously solution template-free self-assembly [40].

4. Conclusions

In summary, crystalline Fe_3O_4 nanoplates were obtained by ultrasonic irradiation in the reaction medium at low temperature within a short reaction time, avoiding deoxygenated conditions and Fe^{2+}/Fe^{3+} molar ratio control. The size of the nanoplates was increased as the initial temperature of the reaction medium increased. Ultrasonic irradiation is demonstrated to be an effective method to prepare two-dimensional magnetite nanoplates.

Acknowledgements

This work was financially supported by Public-benefit Foundation of Science and Technology Department of Zhejiang Province (No. 2010C31112) and Natural Science Foundation of Zhejiang Province (No. Y4080129).

Appendix A. Supplementary data

Supplementary data associated with this article can be found, in the online version, at doi:10.1016/j.ultsonch.2010.12.008.

References

[1] K.C. Chin, G.L. Chong, C.K. Poh, L.H. Van, C.H. Sow, J.Y. Lin, A.T.S. Wee, J. Phys. Chem. C 111 (2007) 9136.
[2] K. Raj, R. Moskowitz, J. Magn. Magn. Mater. 85 (1990) 233.
[3] M.F. Casula, P. Floris, C. Innocenti, A. Lascialfari, M. Marinone, M. Corti, R.A. Sperling, W.J. Parak, C. Sangregorio, Chem. Mater. 22 (2010) 1739.
[4] Y.J. Wu, J.H. Zhang, Y.F. Tong, X.H. Xu, J. Hazard. Mater. 172 (2009) 1640.
[5] S.W. Cao, Y.J. Zhu, M.Y. Ma, L. Li, L. Zhang, J. Phys. Chem. C 112 (2008) 1851.
[6] H. Iida, K. Takayanagi, T. Nakanishi, T. Osaka, J. Colloid Interface Sci. 314 (2007) 274.
[7] J.H. Wu, S.P. Ko, H.L. Liu, S.S. Kim, J.S. Ju, K.K. Young, Colloid. Surf. A 313–314 (2008) 268.
[8] D.C. Niu, Y.S. Li, Z. Ma, H. Diao, J.L. Gu, H.R. Chen, W.R. Zhao, M.L. Ruan, Y.L. Zhang, J.L. Shi, Adv. Funct. Mater. 20 (2010) 773.
[9] W.D. Zhang, H.M. Xiao, L.P. Zhu, S.Y. Fu, J. Alloys Compd. 477 (2009) 736.
[10] D. Amara, I. Felner, I. Nowik, S. Margel, Colloid. Surf. A 339 (2009) 106.
[11] S. Mathur, S. Barth, U. Werner, H.R. Francisco, R.R. Albert, Adv. Mater. 20 (2008) 1550.
[12] A. Yan, X.H. Liu, G.Z. Qiu, N. Zhang, R.R. Shi, R. Yi, M.T. Tang, R.C. Che, Solid State Commun. 144 (2007) 315.
[13] X. Liu, J. Kim, Mater. Lett. 63 (2009) 428.
[14] J. Lu, X.L. Jiao, D.R. Chen, W. Li, J. Phys. Chem. C 113 (2009) 4012.
[15] J. Wang, Y. Wu, Y. Zhu, Mater. Chem. Phys. 106 (2007) 1.
[16] H.F. Zhou, R. Yi, J.H. Li, Y. Su, X.H. Liu, Solid State Sci. 12 (2010) 99.
[17] D. Shi, J.P. Cheng, F. Liu, X.B. Zhang, J. Alloys Compd. 502 (2010) 365.
[18] Y. Mizukoshi, T. Shuto, N. Masahashi, S.J. Tanabe, Ultrason. Sonochem. 16 (2009) 525.
[19] C. KittelL, Phys. Rev. 70 (1946) 965.
[20] C.P. Bean, J.D. Livingston, J. Appl. Phys. 30 (1959) 120S.
[21] R.V. Kumar, Y. Koltypin, X.N. Xu, Y. Yeshurun, A. Gedanken, I. Felner, J. Appl. Phys. 89 (2001) 6324.
[22] J. Wang, Q. Chen, C. Zeng, B. Hou, Adv. Mater. 16 (2004) 137.
[23] Q. Han, Z.H. Liu, Y.Y. Xu, H. Zhang, J. Cryst. Growth 307 (2007) 483.
[24] G.F. Zou, K. Xiong, C.L. Jiang, H. Li, Y. Wang, S.Y. Zhang, Y.T. Qian, Nanotechnology 16 (2005) 1584.
[25] S.H. Xuan, Y.X.J. Wang, J.C. Yu, K.C.F. Leung, Chem. Mater. 21 (2009) 5079.
[26] J.P. Cheng, Z.M. Liao, D. Shi, F. Liu, X.B. Zhang, J. Alloys Compd. 480 (2009) 741.
[27] J.P. Cheng, X.B. Zhang, Z.Q. Luo, Surf. Coat. Technol. 202 (2008) 4681.
[28] F. Dang, N. Enomoto, J. Hojo, K. Enpuku, Chem. Lett. 37 (2008) 530.
[29] F. Dang, N.Y. Enomoto, J.C. Hojo, K.J. Enpuku, Ultrason. Sonochem. 16 (2009) 649.
[30] R.A. Mukh-Qasem, A. Gedanken, J. Colloid Interface Sci. 284 (2005) 489.
[31] S. Zhao, S. Asuha, Powder Technol. 197 (2010) 295.
[32] T. Yamashita, P. Hayes, Appl. Surf. Sci. 254 (2008) 2441.
[33] J.P. Cheng, X.B. Zhang, G.F. Yi, Y. Ye, M.S. Xia, J. Alloys Compd. 455 (2008) 5.
[34] Y. Teraoka, S. Nanri, I. Moriguchi, S. Kagawa, K. Shimanoe, N. Yamazoe, Chem. Lett. 29 (2000) 1202.
[35] M.G. Siles-Dotor, Bokhimi, A. Morales, M. Benaissa, A. Cabral-Prieto, Nanostruct. Mater. 8 (1997) 657.
[36] J.P. Cheng, X.B. Zhang, X.Y. Tao, H.M. Lu, Z.Q. Luo, F. Liu, J. Phys. Chem. B 110 (2006) 10348.
[37] J.P. Cheng, X.B. Zhang, Y. Ye, J. Mater. Process Technol. 206 (2008) 180.
[38] C. Pacholski, A. Kornowski, H. Weller, Angew. Chem. Int. Ed. 41 (2002) 1188.
[39] S. Gustafsson, A. Fornara, K. Petersson, C. Johansson, M. Muhammed, E. Olsson, Cryst. Growth Des. 10 (2010) 2278.
[40] Z.Y. Tang, Z.L. Zhang, Y. Wang, S.C. Glotzer, N.A. Kotov, Science 314 (2006) 274.
[41] J. Wang, Z.M. Peng, Y.J. Huang, Q.W. Chen, J. Cryst. Growth 263 (2004) 616.